Energy & Environmental Science

PAPER

View Article Online
View Journal | View Issue

Cite this: *Energy Environ. Sci.*, 2017, **10**, 1517

Near-complete suppression of surface losses and total internal quantum efficiency in $BiVO_4$ photoanodes†

Bartek J. Trześniewski,[a] Ibadillah A. Digdaya,[a] Tetsuro Nagaki,[a] Sandheep Ravishankar,[b] Isaac Herraiz-Cardona,[b] David A. Vermaas,[a] Alessandro Longo,[cd] Sixto Gimenez[b] and Wilson A. Smith *[a]

Received 19th December 2016,
Accepted 26th May 2017

DOI: 10.1039/c6ee03677e

rsc.li/ees

Bismuth vanadate ($BiVO_4$) is one of the most efficient light absorbing metal oxides for solar water splitting. $BiVO_4$ photoanodes immersed in an electrolyte in an open circuit configuration and exposed to simulated solar illumination for prolonged time achieve superior photoelectrochemical (PEC) activity. This photocharging (PC) effect is capable of almost completely overcoming the surface and bulk limitations of $BiVO_4$. Herein we show that alkaline conditions favor the PC effect; specifically $BiVO_4$ photoanodes subjected to PC treatment at pH 10 achieve a record high photocurrent for undoped and uncatalyzed $BiVO_4$ of 4.3 mA cm^{-2} @ 1.23 V_{RHE}, an outstandingly low onset potential of 0.25 V_{RHE}, and a very steep photocurrent onset. Alkaline conditions also facilitate excellent external and internal quantum efficiencies of 75 and 95% respectively (average in the 440 nm $> \lambda >$ 330 nm range). Moreover, impedance spectroscopy and *in situ* XAS study suggest that electronic, structural and chemical properties of the bulk of these films remain unchanged during the PC treatment. However, appreciable changes in the surface-related properties take place. Ultimately, our results indicate that the improved activity of PC-$BiVO_4$ is enhanced by surface reaction pathways of the semiconductor–liquid junction, which is directly correlated with the electrochemical environment in which it is modified.

Broader context

Photoelectrochemical (PEC) water splitting is an attractive route to capture, convert and store the energy from the sun in the form of chemical bonds. This approach allows for sustainable production of solar fuels (typically H_2), and thereby addresses the challenges of new energy technologies needed in the pathway towards a carbon-free economy. Solar water splitting relies on PEC cells, consisting of semiconducting photoelectrodes, which directly utilise photo-generated charge carriers to drive the water oxidation and reduction half-reactions on the corresponding solid/liquid interfaces. Metal oxides have been heavily studied as a class of photoelectrode materials for PEC devices due to their low cost and stable operation. Specifically, bismuth vanadate ($BiVO_4$) has proven to demonstrate significant activity as a photoanode material. However, due to its inherent bulk- and surface-related limitations, complex strategies such as doping or co-catalysis are typically necessary for $BiVO_4$ to reach high yields for O_2 production. Herein, we investigate photocharging (PC), a simple and novel treatment that can dramatically improve the water splitting capabilities of $BiVO_4$. We demonstrate that illumination combined with alkaline conditions alters the chemistry at the semiconductor–electrolyte interface to form a $BiVO_4$ surface with superior activity for the oxygen evolution reaction.

Introduction

The storage of intrinsically intermittent solar energy in the form of chemical fuels (*e.g.* H_2) has the potential to simultaneously combat global environmental and energy problems. Photoelectrochemical (PEC) water splitting is one of the most promising approaches for such renewable and sustainable production of hydrogen.[1–4] Metal oxides have been extensively used[5] as a promising class of photo-electrode materials for PEC devices, due to their high (photo)chemical stability, abundance and low cost, as well as suitable optical and electronic properties.

[a] *Delft University of Technology, Faculty of Applied Sciences, Department of Chemical Engineering, Materials for Energy Conversion and Storage (MECS), Van der Maasweg 9, 2629 HZ Delft, The Netherlands. E-mail: W.Smith@tudelft.nl*
[b] *Universitat Jaume I, Institute of Advanced Materials (INAM), Av. de Vicent Sos Baynat, s/n, 12071 Castelló de la Plana, Spain*
[c] *Netherlands Organization for Scientific Research (NWO), The European Synchrotron Radiation Facility (ESRF), CS40220, 38043 Grenoble Cedex 9, France*
[d] *ISMN-CNR, UOS Palermo, Via Ugo La Malfa, 153, 90146 Palermo, Italy*

† Electronic supplementary information (ESI) available. See DOI: 10.1039/c6ee03677e

However, out of the wide selection of metal oxides, so far only a few materials, Fe_2O_3,[6] WO_3,[7] $BiVO_4$[8] and Cu_2O,[9] have demonstrated reasonable performance under simulated solar illumination (*i.e.* photocurrent over 2 mA cm^{-2} and a large photovoltage).

Among the metal oxides, bismuth vanadate ($BiVO_4$) is a material with the highest reported solar to hydrogen (STH) conversion efficiency to date (5.2%).[10,11] $BiVO_4$ is an n-type photoanode material, with a bandgap energy of 2.4 eV,[12] and a theoretical efficiency of ~9% STH,[13] is made of cheap, relatively earth abundant, non-toxic elements and is reasonably stable under neutral conditions. However, it suffers from surface and bulk recombination losses that limit its performance to well below its theoretical maximum.[13] The deposition of a co-catalyst (Co–P_i,[13–16] Co–B_i,[17] Ni–B_i,[18] FeOOH/NiOOH,[19] Fe_2O_3/ZrO_2[20]) has been reported to successfully mitigate the surface-related limitations of $BiVO_4$ and has enabled the ability to achieve close to 100% catalytic efficiencies for the oxygen evolution reaction (OER). Complementarily, the low electronic conductivity of $BiVO_4$ has been partially overcome *via* doping with high-valence cations such as W[13,14,21] or Mo[21] which substitute for vanadium. Moreover, fabricating $BiVO_4$ films in a nanostructured morphology has been demonstrated[19,22,23] to overcome the transport limitations caused by the intrinsically short (70 nm)[24] diffusion length of photogenerated charge carriers. Finally, surface passivation of $BiVO_4$ films with thin layers of TiO_2 has also been shown[25,26] to significantly improve its stability. While these techniques are mostly successful in improving the overall PEC activity of $BiVO_4$, they add extra steps to the material processing and introduce significant complexity in optimizing a practical PEC water splitting device.

In our recent work[27] we have reported for the first time on a photoelectrochemical procedure called photocharging (PC), which enables the ability to successfully improve both bulk and surface limitations of $BiVO_4$ photoanodes. We have demonstrated that prolonged exposure of $BiVO_4$ photoanodes in an aqueous solution under open circuit (OC) conditions to simulated solar irradiation can greatly increase its solar water oxidation efficiency *via* a reduced onset potential and an increased maximum photocurrent density. A similar change in various properties of light active materials exposed to illumination has been widely recognized in the photovoltaic (PV) field as a so-called light soaking effect.[28–31] However, to date, no analogous effect has been identified in the PEC field. Moreover, it seems that the mechanism of the photocharging effect observed for $BiVO_4$ may be quite different from PV light soaking. For instance, the light soaking effect observed in PV devices is a purely solid-state phenomenon, *i.e.* it concerns only the interaction between the solid-state materials and the incident electromagnetic radiation. Accordingly, the light soaking effect in the PV cells has been usually ascribed[28–31] to the alteration of the defect structure, change in DOS of trap states or interdiffusion within the light active materials. In contrast, according to our results, the presence of a liquid electrolyte is essential to the PC effect, and no PC can take place without it, *i.e.* the PC effect does not occur when the $BiVO_4$ films are illuminated in air. These findings indicate that the PC effect should be studied in the context of the semiconductor–liquid junction (SLJ), the key interface in a PEC system.[32–36] The significance of the SLJ stands out by the number of important processes in which it is involved: mediation of the transport of charge carriers, formation and passivation of surface states, and catalysis of the oxygen evolution reaction (OER) *via* the formation of reaction intermediates.

Herein we provide new insights into the possible mechanisms of photocharging in $BiVO_4$ photoanodes, and how it directly leads to improved PEC performance. We investigate changes in the PEC, optical, structural, chemical and electronic properties of photocharged $BiVO_4$ in the context of the SLJ, to provide further insights into the chemical and physical mechanisms behind the PC phenomenon. Firstly, we investigate the effect of the electrolyte pH on the PC efficiency as a function of time to understand whether the PC effect is related to the formation of oxy/hydroxyl-based water oxidation intermediates (HO*, O*, HOO*). Since protons/hydroxyl groups are directly involved in all the steps that constitute the OER,[37] we expect that if the PC treatment promotes the formation of any of the water oxidation intermediates, then a different pH could heavily affect the PC efficiency. We show that alkaline conditions favor the PC effect, and specifically that $BiVO_4$ photoanodes subjected to the PC treatment at pH 10 achieve a record high photocurrent for undoped and uncatalyzed $BiVO_4$ of 4.3 mA cm^{-2} @ 1.23 V_{RHE}, an outstandingly low onset potential of 0.25 V_{RHE}, and excellent external and internal quantum efficiencies of 75 and 95% respectively (average in the 440 nm $> \lambda >$ 330 nm range). Secondly, we perform an *in situ* UV-vis spectroscopic study to examine if PC leads to changes in the optoelectronic properties of $BiVO_4$, and hence possibly to different electronic transport properties. We observe that PC leads to increased absorption outside the bandgap energy region of $BiVO_4$ ($\lambda >$ 520 nm), especially under the PC-facilitating alkaline conditions. However, this increased absorption does not seem to be directly responsible for the photocurrent enhancement, since the external quantum efficiency (IPCE) of PC-$BiVO_4$ for $\lambda >$ 520 nm remains negligible. In addition, we use impedance spectroscopy to investigate the effect of PC on the electronic properties of $BiVO_4$ and observe only negligible changes in the bulk electronic properties of $BiVO_4$ films before and after the treatment. However, we observe a significant change in surface-related properties; an increase in capacitance and a decrease in resistance. Lastly, we use *in situ* electrochemical X-ray absorption spectroscopy (XAS) to study the chemical and structural properties of $BiVO_4$ under PEC conditions. Our findings suggest that neither applying a bias potential nor the photocharging treatment alters the structure/chemistry of the bulk of our $BiVO_4$ films; specifically, the oxidation state of vanadium does not seem to change. Overall, our results suggest that PC is related to a light-driven alteration of the surface of $BiVO_4$, and is highly preferential under alkaline conditions. Those changes are most likely related to the formation of highly active water oxidation intermediates and/or changes in the chemistry of the surface. We propose a model in which the surface of $BiVO_4$ becomes hydrogenated under alkaline conditions and under illumination, coupled with creation of oxygen vacancies and reduction of vanadium species,

and possibly accompanied by creation of oxo-water intermediates. Consequently, electrocatalytic properties become more beneficial for solar driven water splitting applications. Furthermore, any bulk-related effects that we identify are mediated by phenomena occurring at the surface, which highlights the importance of the SLJ for the efficiency of PEC devices.

Results and discussion

Influence of pH on PC $BiVO_4$ under illumination

To understand the importance of the SLJ during photocharging treatments, the effect of the electrolyte pH on the PC efficiency was studied first. Fig. 1 presents *J–V* curves of 200 nm thick $BiVO_4$ photoanodes under AM1.5 illumination in PBA buffer at pH 4, 7 and 10 collected before (dashed lines) and after (solid lines) PC for 20 hours. For untreated $BiVO_4$, *J–V* curves recorded at pH 4, 7 and 10 show little difference. Given the sample-to-sample variation, they can be considered similar, though pH 4 gives consistently the lowest activity in terms of photocurrent density. It is apparent that pH has little influence on the photocurrent generation of untreated $BiVO_4$. Consequently, we can conclude that different concentrations of H^+ or OH^- do not significantly influence the light driven oxidation of water on untreated $BiVO_4$ photoanodes.

In contrast, for photocharged $BiVO_4$, *J–V* curves recorded at pH 4, 7 and 10 show striking differences. There seemingly exists a very strong relationship between the alkalinity of the electrolyte and PEC activity of the photocharged electrodes; in particular, a high pH promotes a high photocurrent and a low onset potential. We observe photocurrent densities of 1.0, 3.3 and 4.3 mA cm^{-2} @ 1.23 V_{RHE} at pH 4, 7 and 10 respectively. In our initial study[27] we have reported 3.3 mA cm^{-2} @ 1.23 V_{RHE} at pH 7, herein we were able to achieve 4.3 mA cm^{-2} @ 1.23 V_{RHE} using a pH 10 electrolyte. This is by far the highest reported photocurrent at 1.23 V_{RHE} for undoped and uncatalyzed $BiVO_4$ photoanodes. Moreover, there is also a very clear difference in the slope of the photocurrent in different media. Slightly acidic conditions at pH 4 results in a very sluggish photocurrent onset; initially the *J–V* curve is almost flat and a significant overpotential is required to achieve reasonable photocurrent densities. On the other hand, alkaline conditions at pH 10 lead to a very steep photocurrent onset from the very beginning, with no observable inflection point in the *J–V* curve, a trend more typical for measurements where no surface limitations are present,[38] for example when a sacrificial hole scavenger such as H_2O_2 is employed.[27] The different slopes suggest that alkaline conditions facilitate major suppression of surface recombination[39] in PC $BiVO_4$. Interestingly, the *J–V* curves at pH 4 recorded before and after the PC treatment overlap, showing that at this pH no PC effect takes place. It seems that there is a threshold pH for the PC to take place and under sufficiently acidic conditions (pH < 7) no PC can occur. This implies that a certain concentration of hydroxyl groups is necessary for the PC treatment to be successful.

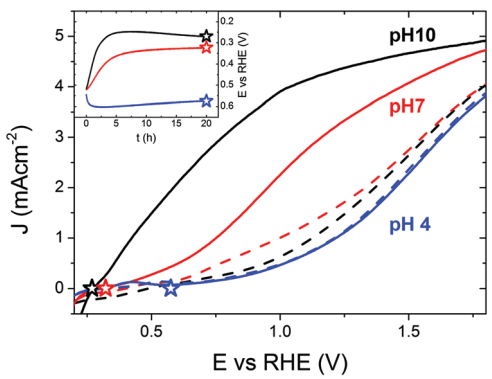

Fig. 1 *J–V* curves of $BiVO_4$ in PBA buffer, pH 4, 7 and 10; a stable 10th anodic scan is shown in each case. Dashed curves – untreated films, solid curves – photocharged films. Each PC treatment was performed in the same pH as the corresponding CV experiment. Inset: *E–t* OC trends collected during the PC treatment. Stars in both plots denote the final photocharging OC potential. Experimental conditions: back-side AM1.5 illumination, films of 200 nm thickness, scan rate of 50 mV s^{-1}.

Moreover it seems that no specific anion or cation is responsible for the PC effect. As presented in S1 (ESI†), electrolytes with compositions different than K-P_i or PBA buffer can successfully facilitate the PC effect, following a pH trend similar to what is demonstrated in Fig. 1. In addition, a series of experiments were conducted to measure the photocurrent density as a function of thickness (S2 (ESI†) black curves). As expected, due to low absorption of $BiVO_4$, the photocurrent density produced by our photoanodes scales up with thickness of the films, up to *ca.* 200 nm limit. There's no significant gain in current for films thicker than 200 nm since 200 nm thick films already absorb most of the available light[40] and going beyond 200 nm may be detrimental due to the 70 nm diffusion length of charge carriers in $BiVO_4$[24] and consequently any gain related to increased absorption could be potentially consumed by bulk transport and recombination losses. S2 (ESI†) also presents the time evolution trends of the PC process (curves red to blue). *JV* curves collected every 2 h show a steady increase in photocurrent, cathodic shift of the photocurrent onset and improvement in the fill-factor. It seems that the biggest changes occur in the first 6 h of the treatment, and further improvements are more moderate.

The inset in Fig. 1 shows the time evolution of the $BiVO_4$ potential *vs.* RHE recorded during the PC treatment at pH 4, 7 and 10. The dark open circuit potentials for each pH are shown in ESI† (S3), where the pH does not show a strong influence ($E_{OC,dark}$). It can be seen that more strongly alkaline pH values favor lower light induced equilibrium potentials (closer to the $BiVO_4$ conduction band-edge). Accordingly, we measured the equilibrium open-circuit (OC) potentials of 0.58, 0.32 and 0.27 V_{RHE} for pH 4, 7 and 10 respectively. Remarkably, the final OC potentials (E_{OC}, marked with stars in both the inset and the main plot) and the photocurrent onset potentials (E_{onset}) seem to be identical for the corresponding pH values. A correlation between E_{OC} and E_{onset} is something to be expected, since measurements of E_{OC} can be used to determine the photovoltage (V_{ph}); any changes in V_{ph} are usually reflected in a shift of E_{onset}[35] since V_{ph} can be simply viewed as the amount of bias

voltage provided by a photoelectrode itself. However, this exact coincidence of the long-term equilibrium OC potential after photocharging and the photocurrent onset potential of the *J–V* curves under solar illumination is a unique feature of our photoanodes. It seems that the onset of PEC activity corresponds directly to the photocharged OC potential, and thus the match between these values shows that there has been a significant reduction in the overpotential required to evolve oxygen in photocharged samples. It may imply very fast exchange current densities at the SLJ. Importantly, this proposed correlation seems to hold in the whole pH 4–10 range, and is therefore not a signature of PC-enhanced performance, but rather a unique feature of our material. Notably, measurements collected at different pH values have very different photocurrent slopes at the onset: very sluggish at pH 4 and very steep at pH 10. Therefore, while the exchange current densities may be very fast in the whole pH range, the losses at the interface still vary significantly depending on the pH. To further prove that the OC potential under illumination correlates directly with the OER onset potential, we performed an $i(t)$ experiment at a potential slightly (0.1 V) above the OC potential of a photocharged $BiVO_4$ anode (S4 and S5, ESI†). Our results show that a small anodic bias of 0.1 V *vs.* the OCV (potential too low to drive OER on untreated $BiVO_4$, see S6 and S7, ESI†) can result in some non-negligible current over 30 hours, suggesting that the observed current is indeed related to the OER.

The potential of a photoelectrode probed by a potentiostat can be considered to be equivalent to its Fermi level position E_F or quasi-Fermi level position of the electrons $E_{F,n}$.[36] While the OC potential measured by the potentiostat corresponds effectively to the back contact and not to the surface, it is assumed that any change in one would trigger a similar change in the other. Therefore, we consider the '*E vs. t*' measurements (Fig. 1, inset) as a technique to monitor *in situ* the effect of the PC treatment on the $E_{F,n}$ of $BiVO_4$. Our data show that under PC conditions facilitating the highest enhancement in the photocurrent (pH 10), the OC potential strongly shifts towards the water reduction potential (0 V_{RHE}) during the PC time (Fig. 1, inset, black curve). Therefore, we can conclude that a successful PC treatment leads to a shift of the $BiVO_4$ $E_{F,n}$ towards the conduction band edge.

The observed shift in the OC potential can be related to pinning of the electron Fermi level by the surface capacitive layer. Pinning of E_F has been reported to have a strong effect on the obtainable photovoltage (V_{ph}).[35,36,41] Our previous results[27] suggest that the photocharging treatment may be related to changes in the chemical compositions of the surface. Consequently the surface of $BiVO_4$ altered during the photocharging seems to give rise to an energetic level at which the Fermi level pins. Our data indicate that Fermi level pinning at the energy level related to this newly formed capacitive layer is more beneficial for water oxidation *via* an increase of V_{ph}. Furthermore, it has been proposed that under heavy Fermi level pinning conditions, an extra bias voltage may be necessary to start driving the OER.[42] This agrees well with our *J–V* data, which shows that the overpotential to drive OER with untreated $BiVO_4$ is significantly higher than those for photocharged films (supposedly diminished Fermi level pinning). The electronic properties of this proposed surface capacitive layer are further discussed in the impedance spectroscopy section.

One other possible explanation of this OC potential shift could be related to the formation of some oxy/hydroxyl-based water oxidation intermediates at the surface of $BiVO_4$. In general, the chemical nature of the surface adsorbates can be expected to depend strongly on the electrolyte properties. Specifically, in water based electrolytes, the pH will heavily affect the type of aqueous-based adsorbates on the surface of a photoelectrode. Correspondingly, the properties of the SLJ, in particular the surface adsorbates, can affect in some way the chemical reaction mediated by the surface, in our case water oxidation. It seems plausible that under alkaline conditions, high OH^- concentration produces adsorbates that can be readily transformed with the charge carriers excited during the PC treatment into more active water oxidation intermediates, simultaneously resulting in an altered $E_{F,n}$. Importantly, it has been proposed[36] that the adsorption of H_2O molecules and its derivatives is responsible for the surface states observed typically on MO_x photoanodes. Therefore, both presented hypotheses may in fact share a common mechanism.

Furthermore, on the contrary to what has been recently reported,[43] our $BiVO_4$ photoanodes do not show any changes in PEC activity when subjected to prolonged illumination in air (S8, ESI†), establishing the necessity of the electrolyte to facilitate the PC effect. Clearly, different deposition techniques used to fabricate $BiVO_4$ films (spin coating in Berlinguette's work[43] and spray pyrolysis in our case) inevitably produce films of different compositions and different defect structures, which is further supported by our XPS study presented in Fig. 2. In the work of Berlinguette, a strong peak at ca 532 eV can be observed for untreated samples, which is ascribed to surface defect sites (*e.g.*, dangling oxo or hydroxy groups). However, we observe exactly the opposite; our initial material demonstrates a relatively weak signal at 532 eV. Further on, since the starting material is quite different, we believe that both treatments lead to a different modification and facilitate some different chemical transformation at the surface. In the work of Berlinguette the oxygen peak at 532 eV diminishes over the UV-curing treatment time, which is

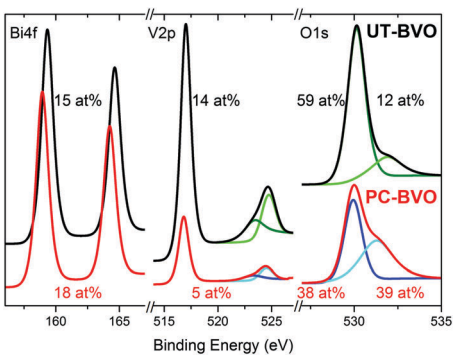

Fig. 2 XPS spectra of $BiVO_4$ photoanodes before and after photocharging in 0.1 M PBA buffer, pH 10, under AM1.5G simulated illumination.

ascribed to removal of the surface states. On the contrary, we observe that it is only once the oxygen peak at 532 eV becomes more pronounced that an enhanced activity for photoelectrochemical water oxidation by our photoanodes can be achieved. We tentatively ascribe this 532 eV peak to hydroxyl groups.[44] Moreover, we observe a significant decrease in the surface vanadium concentration of photoanodes subjected to photocharging treatment. Overall, our XPS study clearly demonstrates that our initial material is different from that of Berlinguette and that we are driving a different chemical transformation with our photocharging treatment. The surface of the photocharged $BiVO_4$ seems to be terminated with some extra hydroxyl groups, to have a decreased concentration of vanadium and to be enriched with oxygen, which happens to make it more active for OER.

Spectroscopic study of PC $BiVO_4$

To further probe the optoelectronic properties of $BiVO_4$ photoanodes during photocharging, we performed *in situ* UV-vis spectroscopy to measure the change in optical transmittance of the photoanodes during electrochemical testing. Fig. 3 shows the change in transmittance of the films at 550 nm (above the 520 nm bandgap of $BiVO_4$), collected *in situ* during the PC process. It was observed that for all the 3 pH values studied, the PC treatment leads to a gradual decrease in transmittance at 550 nm, meaning more absorption in the above bandgap region. Moreover, we detect a strong change in transmittance at pH 10 and a very slight one at pH 4. Therefore, regardless of the mechanism for this optical change, the hydroxyl groups seem to be facilitating the darkening effect.

Our spectral data suggest that there is a direct correlation between the pH and strength of the observed optical effect, *i.e.* alkaline conditions favor the darkening of $BiVO_4$ outside the band gap region. In the previous section we identified a similar correlation between the electrolyte pH and the strength of the PC effect, *i.e.* the higher the pH the more the photocurrent extracted from a photocharged $BiVO_4$ sample. This implies that a 'darker state' of $BiVO_4$ can be associated with higher photocurrents. However, there is no clear plateau in the $\Delta T/dt$ trend, suggesting that a full transition to a 'darker state' is not a necessary condition to fully photocharge $BiVO_4$.

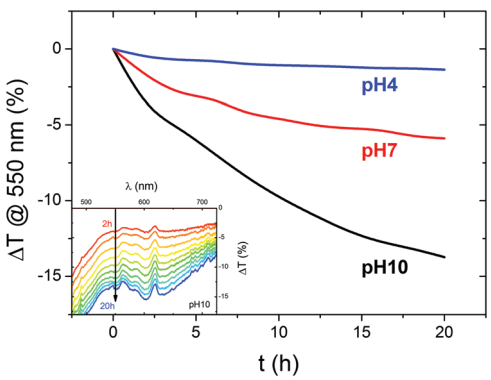

Fig. 3 Relative change in optical transmittance at 550 nm wavelength as a function of PC time of $BiVO_4$ in PBA buffer, pH 4, 7 and 10. Inset – relative change in optical transmittance in the above-bandgap spectral range as a function of PC time of $BiVO_4$ in PBA buffer, pH 10, shown with a time step of 2 h, the arrow indicates the trend.

To understand whether the extra above-the-bandgap absorption of photocharged $BiVO_4$ yields an improved photocurrent density, *i.e.* if it creates charge carriers useful for water oxidation, external quantum efficiency (EQE), or incident photon to current conversion efficiency (IPCE) experiments were performed. Fig. 4(a) shows the results of the EQE measurements of $BiVO_4$ photoanodes before and after PC. All the EQE curves show the onset of the photocurrent at a wavelength of about 520 nm, in good agreement with the bandgap energy of 2.4 eV typically reported for $BiVO_4$.[12] All the curves reach a quasi-plateau at a wavelength of about 440 nm. This slow rise in EQE is a direct consequence of optical properties of $BiVO_4$. It is widely believed that a range of weak valence to conduction band transitions in the near bandgap wavelength range[45] is responsible for a slow rise in the absorption coefficient of $BiVO_4$, and consequently the observed trend in EQE.

Our EQE results clearly show that PC has a remarkable impact on the quantum efficiency of $BiVO_4$ photoanodes. Untreated $BiVO_4$ demonstrates an average IPCE of 20%, while PC $BiVO_4$ shows average IPCE of 75% and 50% for pH 10 and pH 7 respectively ($440\ nm > \lambda > 330\ nm$ range). The EQE results follow a trend similar to the voltammetry measurements, *i.e.* a high pH favors a high quantum efficiency. Fig. 4(b) presents the internal quantum efficiency (IQE), or absorbed photon to current conversion efficiency (APCE) data obtained by integrating the absorption spectra of the films with the EQE/IPCE. For pH 10, we can calculate the average internal quantum efficiency to be around 95% in the 330 to 440 nm wavelength range. This remarkable result clearly shows that the PC treatment allows our $BiVO_4$ photoanodes to convert almost all of the absorbed photons into extractable photocurrent, suggesting that the PC treatment at pH 10 can eliminate both catalytic and bulk limitations almost entirely. This is an unprecedented result for a non-doped, non-catalyst modified photoelectrode, and represents a benchmark for photo-to-chemical conversion for solar water oxidation.

To further strengthen our claim about near complete suppression of surface losses we also present the catalytic efficiency trends of our $BiVO_4$ photoanodes as a function of potential under different conditions (S9, ESI†). We believe that the observed near unity quantum efficiency is also facilitated by the morphology of our films. Although the investigated photoanodes are 200 nm thick, they're not fully compact and flat. As demonstrated in S10 (ESI†), $BiVO_4$ films fabricated *via* spray pyrolysis are highly porous and intrinsically nanostructured, such that the distance for the charge carriers to travel is significantly less than 200 nm and close to the diffusion length of photogenerated charge carriers reported for $BiVO_4$ (70 nm). Furthermore, it is also possible that the photocharging treatment positively affects the diffusion length of the charge carriers in $BiVO_4$, without affecting the surface morphology at any pH (S10, ESI†).

Interestingly, the quantum efficiency in the above-bandgap wavelength region remains zero after PC. Therefore we can

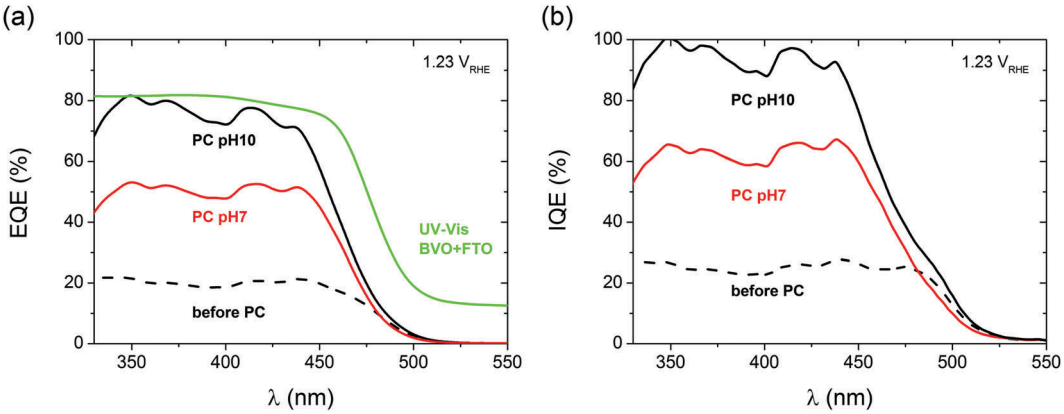

Fig. 4 (a) External and (b) internal quantum efficiency measurements of 200 nm $BiVO_4$ in PBA buffer, pH 7 and 10, before and after PC collected at 1.23 V_{RHE} bias voltage. Green curve – absorption trend of a $BiVO_4$–FTO sample.

conclude that the additional portion of light absorbed by PC $BiVO_4$ in the above-bandgap region, demonstrated as the previously described darkening effect, does not contribute to the increased photocurrent. Increased absorption in the above-bandgap range and unchanged EQE onset could suggest incorporation of H into the near surface layer of our films, since similar optical effects have been reported for hydrogenated $BiVO_4$.[46] Likewise, the darkening effect could possibly be explained by reduction of vanadium species in $BiVO_4$, similarly to what has been reported by Qin *et al.*,[47] who observed enhanced absorption beyond the bandgap in reduced monoclinic $BiVO_4$.

The most likely way for hydrogen to get incorporated into the $BiVO_4$ lattice is *via* intercalation into interstitial sites,[46] leading to the formation of positively charged $\left(H_i^{\bullet}\right)$ defects. For the sake of conservation of charge, it is possible that the formation of those interstitial hydrogen impurities is accompanied by reduction of vanadium, leading to the formation of negatively charged vanadium species $\left(V_V^{'}\right)$. This mechanism is consistent with the XPS study of PC-$BiVO_4$ which we have presented in our initial report,[27] and which shows that surface vanadium undergoes reduction from the 5+ to the 4+ oxidation state during the PC treatment. If we now consider self-doping of the V_2O_5 sublattice with VO_2 species, we may expect that oxygen ions will occupy four out of five oxygen sites in the V_2O_5 sublattice $(O_O^{\times})$, leaving the fifth oxygen site empty and leading to the formation of an oxygen vacancy $\left(V_O^{\bullet\bullet}\right)$. In this particular case special care needs to be taken in order not to confuse the vanadium and vacancy descriptor ($V_V^{'}$ and $V_O^{\bullet\bullet}$). Overall, we can propose the mechanism of light-triggered hydrogenation of the $BiVO_4$ surface layer coupled with the reduction of vanadium surface species; eqn (1) illustrates the possible defect chemistry reaction using the Kröger–Vink notation:

$$2VO_2 + OH^- + 2h^{\bullet} \xrightarrow{V_2O_5} 2V_v^{'} + 4O_O^{\times} + V_O^{\bullet\bullet} + H_i^{\bullet} + 0.5O_2(g) \quad (1)$$

Since our experimental results indicate that both light and alkaline conditions are critical for the PC effect to take place, photogenerated holes ($h^{\bullet}$) and hydroxyl groups (OH^-) are included as reactants with VO_2. The alteration of the surface chemistry *via* the formation of hydrogen interstitials and oxygen vacancies could lead to increased absorption outside the $BiVO_4$ band gap energy and improve the catalytic properties of our photoanodes, which is in agreement with the results from Wang *et al.*,[46] which show that hydrogen treatment leads to improved photocurrents in $BiVO_4$ photoanodes.

In situ X-ray absorption spectroscopy (XAS)

It is unclear whether the whole bulk of $BiVO_4$ films becomes affected by the photocharging treatment. Therefore, in order to investigate any possible impact of the PC treatment on the chemical and structural properties of bulk $BiVO_4$, specifically to identify any changes in the average bulk oxidation state of vanadium and in the local environment, we performed an *in situ* XAS study.

Fig. 5 presents vanadium K-edge XAS spectra collected *in situ* as functions of the (a) PC treatment time and (b) applied bias potential. For $BiVO_4$ films subjected to the PC treatment for 8 h, no changes in the XAS spectrum were observed throughout the experiment. Likewise, *ex situ* conditions and dark OC conditions yield the same spectra (Fig. 5(a)). Similarly, for $BiVO_4$ films poised at potentials of 0.3, 0.7 and 1.1 V_{RHE} there was essentially no shift in the XANES edge energy (Fig. 5(b)). Ultimately, under all the studied experimental conditions, the XAS spectra in the XANES range show a nearly perfect overlap. Therefore, we conclude that neither the photocharging treatment nor applying bias potentials (0.3–1.1 V_{RHE}) alters the structure/chemistry of the bulk of $BiVO_4$ films; specifically, our films do not display any signatures of changes in the average bulk vanadium oxidation state, despite possessing significantly different PEC properties.

Fig. 5 also includes reference spectra of V_2O_3, VO_2 and V_2O_5. Clearly, the edge position of vanadium oxides shifts to higher energies with increased formal oxidation state (approx. 5470, 5474 and 5476 eV for V^{3+}, V^{4+} and V^{5+} respectively). Based on the spectra of vanadium oxides the oxidation state of V in the $BiVO_4$ films was estimated. Notably, the edge position of a XANES

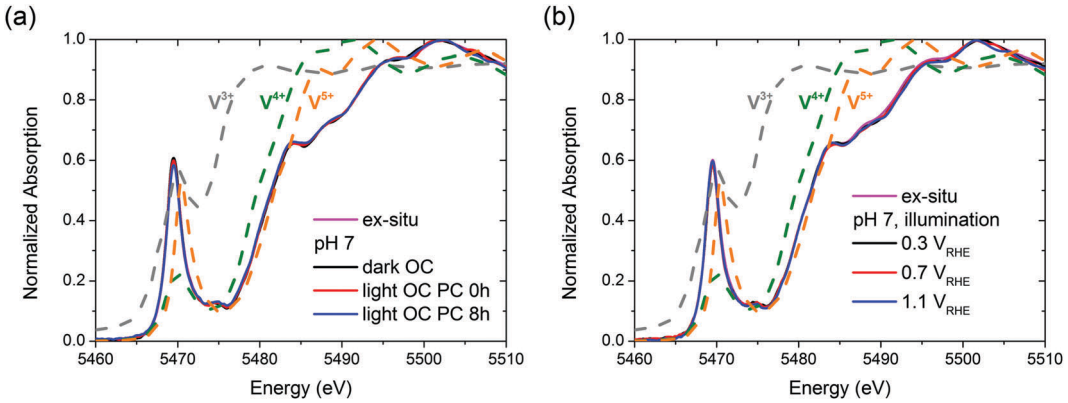

Fig. 5 Vanadium K-edge XAS spectra collected (a) *ex situ* and *in situ* under OC conditions, in the dark and under illumination; (b) *ex situ* and under illumination and with applied bias potentials.

spectrum is only an approximate indicator of the oxidation state of metals owing to the several parameters that contribute to the XANES spectra (*i.e.*, charge density, ligand symmetry, and spin density).[48,49] However, given significant differences between edge positions of different vanadium oxides and a similar chemical environment of vanadium atoms both in VO_x and in $BiVO_4$, the oxidation state of V in our films can be determined quite confidently. The edge position of the $BiVO_4$ films is similar to that of V_2O_5, indicating a mean oxidation state of +5. Since, as discussed in the previous paragraph, all the $BiVO_4$ XAS spectra are essentially the same, we can conclude that bulk vanadium in our films always preserves the +5 oxidation state.

To verify the local arrangement of vanadium in our films and to monitor any possible changes in the spectrum, XANES calculations have been performed. $BiVO_4$ is known to exist in three polymorphs: orthorhombic pucherite, tetragonal dreyerite, and monoclinic clinobisvanite. However, the only thermodynamically stable phase is clinobisvanite. According to the simulations presented in S11 (ESI†) the main atomic arrangement shown by our films is typical of the crystallographic structure of clinobisvanite. Therefore, we can further confirm that bulk vanadium in our films has a dominant oxidation state of +5.

Impedance spectroscopy (IS)

In an effort to find the correlation between the photocharging treatment and charge transfer behavior, we performed cyclic voltammetry (CV) on the untreated (UT) and photocharged (PC) $BiVO_4$, as shown in Fig. 6. In the presence of trap states (*i.e.*, surface states), one or more reduction peaks are usually present in the cathodic voltammetry scan, which can be attributed to charging or filling of electrons from the conduction band to the surface state as the electron Fermi level shifts upward during the cathodic sweep.[50–52] In the dark voltammetry, thus in the absence of photogenerated holes, such trap-related reduction peaks are irreversible. The irreversibility of these capacitive cathodic peaks has been related to the equilibration between the trap states and conduction band.[52] In order to unambiguously identify any trap-related peaks, the CV is typically performed in the dark, to avoid masking the possible trap capacitive effects by the photocurrent. The CV scan of the UT sample shown in Fig. 6(a) depicts both anodic and cathodic peaks, which cannot be assigned to deep surface traps (which are irreversible). The reversible peaks, however, can be ascribed to the reduction and re-oxidation of the redox system of V^{5+} to V^{4+}. It is noticeable that these redox peaks are barely visible in the dark and significantly

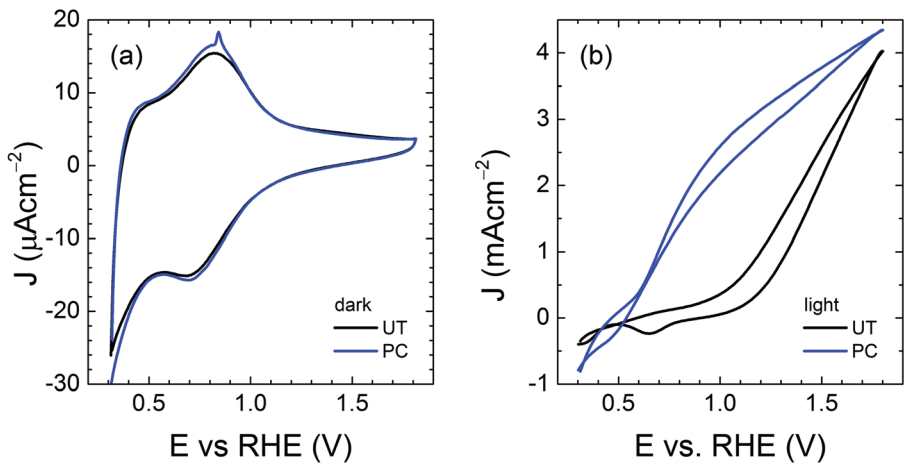

Fig. 6 Cyclic voltammetry of untreated (UT) and photocharged (PC) $BiVO_4$ (a) in the dark and (b) under illumination.

more pronounced under illumination (S12, ESI†), since the photogenerated charge also contributes to the oxidation and reduction of these redox states. Moreover, slightly higher capacitance can be derived from the hysteresis of the PC cyclic voltammetry curve in Fig. 6(a).

Consequently, we carried out impedance spectroscopy (IS) measurements to characterize the carrier dynamics in the bulk and on the surface of the untreated (UT) and photocharged (PC) $BiVO_4$ in the dark and under illumination using physical models (*i.e.*, equivalent circuit, EC) that have been used extensively for n-type metal oxide semiconductors when surface states are present (see S13, ESI†).[53–55] Fig. 7(a) shows the bulk capacitance of UT and PC $BiVO_4$ in the dark and under illumination as a function of applied potentials obtained from the IS measurements. This capacitance shows a peak at *ca.* 0.7 V_{RHE} which increases both under illumination and after the PC treatment. This behavior is consistent with the cyclic voltammetry study demonstrated in Fig. 6 and Fig. S12 (ESI†), and can be ascribed to the redox process of V^{4+}/V^{5+}. However, we found that the photocharging treatment involving reduction of V^{5+} to V^{4+} does not affect the bulk electronic properties, as indicated by the constant bulk resistance for the untreated and the photocharged samples, shown in Fig. 7(b). This likely suggests that the onset potential shift and increase of the photocurrent observed in our photocharged samples are not related to the bulk conductivity of the material.

Further on, we looked for signatures of any changes in the band structure of $BiVO_4$ occurring during the photocharging process. Fig. 7(c) presents the bulk capacitance *versus* applied voltage, plotted as a Mott–Schottky dependence. The Mott–Schottky plot allows for estimation of the flat band potential (V_{fb}) of our samples. Due to a significant overlap of the redox capacitance (the peak at 0.7 V_{RHE}) with the space charge capacitance of $BiVO_4$, the potential window available for the linear Mott–Schottky dependence is very narrow. However, the extraction of the space charge capacitance is still possible, as shown in Fig. 7(d). We noticed that the flat band potential shifts anodically upon photocharging treatment, which is consistent with hole accumulation at the capacitive layer. In any case, the positive shift does not contribute to the cathodic shift of the photocurrent onset potential of the photocharged $BiVO_4$. This cathodic shift of the photocurrent is related to reduced surface recombination, improving the performance of the photoanodes.

The IS response of illuminated $BiVO_4$ photoanodes also showed some distinctive feature in the low frequency regime. Such a feature can be usually attributed to a surface signature, such as charging/discharging of the surface states[54] and/or catalytic layers.[55,56] In order to properly address this phenomenon, the

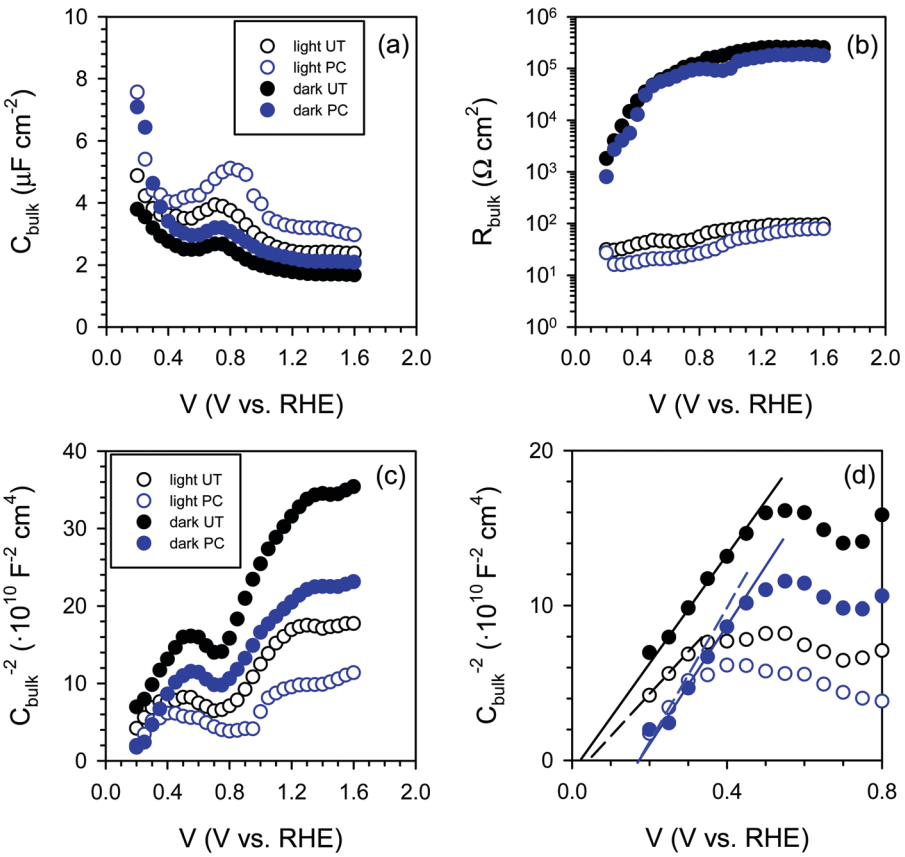

Fig. 7 (a) Bulk capacitance (C_{bulk}) and (b) bulk resistance (R_{bulk}) as a function of potential, (c and d) Mott–Schottky plots obtained in the dark and under illumination under different PC conditions measured at pH 10.

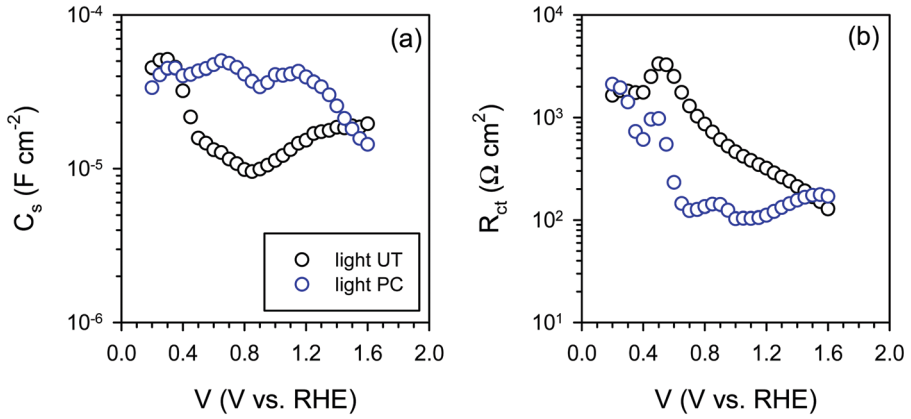

Fig. 8 (a) Surface capacitance (C_s) and (b) charge transfer resistance (R_{ct}) of the untreated (UT) and the photocharged (PC) $BiVO_4$ under illumination at pH 10.

evolution of both surface capacitance (C_s) and charge transfer resistance (R_{ct}) with potential was studied, as depicted in Fig. 8. From Fig. 8(a) we note that the values of the surface capacitance increase on the photocharged sample, suggesting that surface modification indeed took place during the photocharging treatment. The surface capacitance of PC samples does not demonstrate the typical Gaussian distribution that is generally obtained for a system containing localized surface states.[54,57] In fact, it remains almost constant in a wide potential window (*ca.* 1 V), which is similar to that reported in water splitting systems when a catalytic layer is deposited on the surface of a photoanode.[55,56] Hence, we attribute this capacitance to the formation of a surface layer formed by the photocharging process due to the adsorption of oxy/hydroxyl species as previously discussed, rather than a localized surface trap. This hypothesis is further supported by the evolution of charge transfer resistance shown in Fig. 8(b). The resistance does not significantly evolve over a large potential window and its minima do not correspond to the maxima of the surface capacitance as expected for a surface trap. The surface capacitive layer pins the electron Fermi level which leads to the anodic shift of the flatband potential as observed from Fig. 7(c) for the photocharged samples.

This has been illustrated in the cartoon of Fig. 9, highlighting the proposed mechanisms involved in the photocharging process: intercalation of hydrogen and reduction of surface vanadium favoured under alkaline conditions and formation of the capacitive layer. In the mechanistic cartoon of Fig. 9, the reduced band bending in the photocharged material is due to the shift of the Fermi level towards the conduction band of $BiVO_4$, as a result of the photocharging effect. The shift of the flatband potential to positive potentials is consistent with the accumulation of holes at the interface. The diagram also depicts the increase in the photovoltage of PC $BiVO_4$ (V_{ph2}) *vs.* the photovoltage of the untreated material.

Though the flatband potential moves to more anodic potentials, the capacitive layer acts as a 'hole reservoir' and minimises recombination, leading to an onset potential of about 0.4 V *vs.* V_{RHE}, as observed from Fig. 6(b). From this study it can be concluded that the photocharging treatment accelerates the creation of the OER intermediates on the $BiVO_4$ surface which act as a hole reservoir, in the same manner as a catalytic layer. The origin of this early formation of reaction promoters can be connected to the V^{5+} reduction process under favourable pH electrolyte conditions. The mechanism of the photocatalytic effect by the existence of V^{4+} has been largely described on V

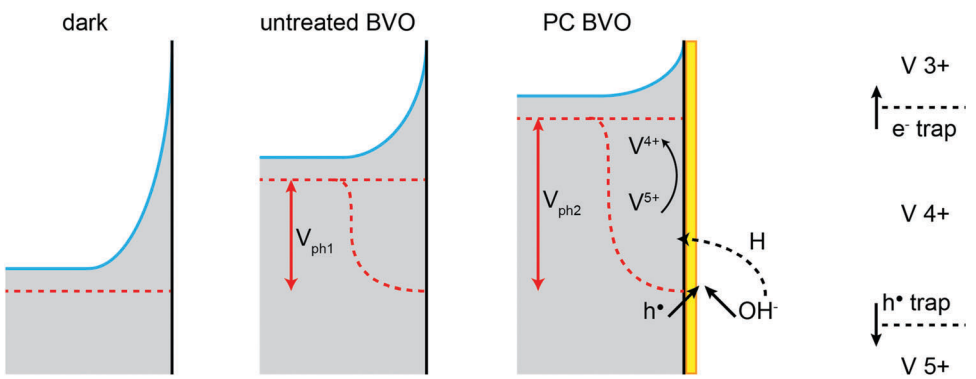

Fig. 9 Band diagrams of $BiVO_4$ in the dark and under illumination before and after the photocharging treatment, including the simplified photocharging mechanism model. The green star indicates the energetic level related to the surface capacitive layer, causing the Fermi level pinning.

multiple valence materials such as V_2O_5 doped TiO_2, CaV_2O_6 and $BiVO_4$ nanorods.[58–60] Furthermore, it has been demonstrated on $BiVO_4$ nanorods that the presence of V^{4+} defects induce oxygen vacancies (V_O) on the surface of nanoparticles.[60] V_O can strongly adsorb O^{2-} and OH^- species on the surface, which leads to an enhanced photocatalytic effect.

To further elucidate the capacitive behavior of our photoanodes, a chopped light chronoamperometry experiment was performed. A similar study[55] has demonstrated that Co–P_i deposited onto α-Fe_2O_3 can efficiently collect and store photogenerated holes from the hematite electrodes. Co–P_i layers of different thicknesses have different charge storage capacities and therefore demonstrate different decay times in chopped light transients. An analogous study performed on Fh/Ta_3N_5[61] describes a ''surface charging'' process, demonstrated by an increase in the photocurrent. This effect is attributed to accumulation of surface trapped holes, resulting in the enhancement of photocurrent. S14 and S15 (ESI†) present respectively the anodic and cathodic transients of the untreated and photocharged $BiVO_4$ photoanodes. The fast decay observed for the untreated films (S14(a), ESI†) could suggest[55] hole accumulation/trapping, charging of the surface states or oxidation of some surface species. On the other hand, photocharged films demonstrate a build-up of photocurrent (S14(b), ESI†), which suggests[61] a capacitance-related effect such as surface charging. Cathodic transients show much faster decay in the case of untreated $BiVO_4$ (S15(a), ESI†), when compared with the photocharged material (S15(b), ESI†). It could be indicative of the higher charge storage capacity of PC-$BiVO_4$, in agreement with our EIS results. Overall, photocharged $BiVO_4$ seems to demonstrate some traits typical of catalyzed photoanodes.

A more in depth analysis of the anodic transients is troublesome since within the potential range used in our study the capacitive and faradaic currents are convoluted, therefore it is difficult to extract the integrated capacitive charge. However, the total charge stored in the case of the cathodic transients can be calculated using eqn (2):

$$\Delta Q = \int J \mathrm{d}t \tag{2}$$

From the observation of the transients, it is clear that higher charge is accumulated at the PC specimens. Further on, the surface capacitance can be calculated using eqn (3):

$$C_s = \frac{\mathrm{d}\Delta Q}{\mathrm{d}E} \tag{3}$$

The capacitance values based on cathodic transients presented in S15 (ESI†) and obtained using eqn (2) and (3) are 0.05 and 0.4 mF cm^{-2} for the untreated and photocharged materials respectively. These values confirm significant differences in the charge storage capabilities of $BiVO_4$ before and after the PC treatment, and are in agreement with the qualitative trends presented in Fig. 8(a).

Conclusions

$BiVO_4$ photoanodes immersed in an electrolyte in the OC configuration and exposed to simulated solar illumination for prolonged time achieve superior PEC activity. This photocharging effect is capable of dramatically improving both bulk and surface functionalities of $BiVO_4$. New insights into the mechanisms of PC in $BiVO_4$ photoanodes and how it leads to improved PEC performance are necessary for its application in real devices.

There seems to exist a strong correlation between the pH of the electrolyte and PEC properties of PC $BiVO_4$: alkaline conditions facilitate the PC effect while acidic conditions prevent it from happening. Specifically PC performed under alkaline conditions at pH 10 yields high photocurrents, low onsets and high fill-factors, as well as very high quantum efficiencies (near 100% internal quantum efficiency), suggesting that both bulk and surface limitations of $BiVO_4$ can be overcome with PC alone. The strong pH dependence of the PC effect suggests that the SLJ plays a key role in the PC mechanism.

The IS study reveals that the photocharging effect is connected with the development of a capacitive layer, which has the ability to accumulate holes, and hence leads to reduced surface recombination. In addition, optical properties of $BiVO_4$ subjected to the PC treatment change, namely, PC $BiVO_4$ starts to absorb light beyond the bandgap range. However, this apparent increase in absorption does not lead to the formation of charge carriers useful for water oxidation but it is rather a signature of the transformation of the material into a more PEC active state. This darkening effect could be potentially related to the intercalation of hydrogen in conjunction with the reduction of vanadium in the surface layer of the films. Importantly, *in situ* XAS study quite convincingly rules out the possibility that the PC treatment leads to reduction of vanadium from the 5+ to the 4+ state within the whole bulk of the films.

Overall, our results suggest that PC is related to light-driven alteration of the surface of $BiVO_4$, preferentially under alkaline conditions. Those changes result in properties becoming more beneficial for solar driven water splitting applications. Furthermore, any bulk-related effects are mediated by phenomena occurring at the surface, which highlights the importance of the SLJ for the efficiency of PEC devices. From a technological perspective, the advantages of the PC effect can be fully exploited under continuous operation of a $BiVO_4$-based photoelectrochemical device, and consequently, redesign of the operation protocols of these devices is imperative to successfully implement this PC effect.

Experimental

Preparation of $BiVO_4$ thin film photoanodes

Thin films of 50, 100, 200 and 300 nm thick $BiVO_4$ were prepared by spray pyrolysis on FTO coated glass substrates. Details of the deposition procedure are described elsewhere[13,16] and are also available in the ESI.† Prior to deposition of $BiVO_4$, a SnO_2 interfacial layer ($\sim$80 nm) was deposited onto the FTO substrate at 425 °C to prevent recombination at the FTO/$BiVO_4$ interface.[62] The substrate temperature during spraying of

$BiVO_4$ was maintained at 450 °C. After deposition, the samples were further annealed for 2 h in a tube furnace at 450 °C in air.

Photoelectrochemical (PEC) measurements

A 0.1 M phosphate buffer (K-P_i) and a 0.1 M phosphate-borate-acetate (PBA) buffer were used as the electrolyte. K-P_i was prepared by dissolving a mixture of KH_2PO_4 (Sigma Aldrich, 99.0%) and K_2HPO_4 (Sigma Aldrich, 99.0%) in Milli-Q water (18.2 MΩ cm), to obtain pH 7.2 and to preserve 0.1 M overall concentration of $PO4^{3-}$. PBA buffer was prepared by dissolving KH_2PO_4 (Sigma Aldrich, 99.0%), H_3BO_3 (Sigma Aldrich, 99.5%) and acetic acid (Sigma Aldrich, 99.7%) in Milli-Q water (18.2 MΩ cm). The concentration of each component was set to 0.1 M. The pH was adjusted to a desired value by titrating the PBA solution with KOH (Sigma Aldrich, 99%), and with a pH meter immersed. Throughout this work the PBA buffer, pH 4, 7 and 10, was used.

PEC characterization of $BiVO_4$ photoanodes was carried out in an electrochemical cell using a three-electrode configuration. The potential of the working electrode was controlled by a multi-channel potentiostat (Parstat MC, Princeton Applied Research). An Ag/AgCl electrode (XR300, saturated KCl + AgCl solution (KS120), Radiometer Analytical) and a coiled Pt wire were used as the reference and counter electrodes, respectively. Measurements under illumination were performed with a Newport Sol3A Class AAA solar simulator (type 94023A-SR3) producing simulated AM1.5 solar illumination (100 mW cm^{-2}). In all the experiments involving illumination, $BiVO_4$ samples were illuminated from the back-side, *i.e.* the light came through the substrate side first. Cyclic voltammetry scans were taken at a scan rate of 50 mV s^{-1} unless stated otherwise.

The photocharging of $BiVO_4$ photoanodes was performed under OC conditions under illumination. $BiVO_4$ samples were placed in the electrochemical cell and exposed to AM1.5 light until the plateau of $V_{WE}(t)$ was reached (10 hours on average).

In situ UV-vis spectroscopy

The spectral data were collected using an OceanOpics USB2000+ spectroradiometer and the SpectraSuite software. The spectroradiometer was placed behind the cell to measure the intensity of light transmitted through a $BiVO_4$ sample.

Quantum efficiency

Monochromatic photocurrents were measured with a 300 W Xe lamp (Oriel LSE340 interface, LSH302 lamp housing, LSN252 power supply, LSB530 lightbulb) coupled into a grating monochromator (ActonSpectraPro 150i). An electronic shutter (Uniblitz LS6) was used, and a long-pass colored glass filter (Schott, 3 mm thick) was placed between the monochromator and the sample to remove second-order diffracted light. The shutter was actuated every 10 s, and the photocurrent was taken as the difference between the current when the shutter is opened and closed (3 s integration time and ~1.5 nm step size). The light intensity was measured with a calibrated photodiode (Ophir PD300-UV) and ranged between 0.3 and 8 mW cm^{-2}. The incident photon to current efficiency (IPCE, sometimes called the external quantum efficiency or EQE) was calculated based on formula (2):

$$\mathrm{IPCE}(\lambda) = \frac{1240(V \times \mathrm{nm}) \times J\,(\mathrm{mA\,cm^{-2}})}{P\,(\mathrm{mW\,cm^{-2}}) \times \lambda\,(\mathrm{nm})} \qquad (4)$$

X-ray absorption spectroscopy (XAS): X-ray absorption near edge structure (XANES) and extended X-ray absorption fine structure (EXAFS)

V K-edge (5465 eV) XAFS spectra of the thin films of $BiVO_4$ were collected at the Dutch-Belgian Beam Line (DUBBLE) at the European Synchrotron Radiation Facility (ESRF).[63] The energy of the X-ray beam was tuned by a double-crystal monochromator operating in fixed-exit mode using a Si(111) crystal pair. All the measurements were performed at ambient temperature and pressure. Spectra of vanadium foil needed for energy calibration and reference spectra of vanadium oxides (V_2O_3, VO_2 and V_2O_5) were collected in transmission mode using Ar/He-filled ionization chambers. EXAFS spectra of the thin films of $BiVO_4$ were collected in fluorescence mode using a 9-element Ge detector (Ortec Inc.).

The XAS investigation of $BiVO_4$ was performed using a cell specially designed for *in situ* PEC measurements. For the sake of probing the vanadium K-edge, characterized with a relatively low energy of 5465 eV, the electrolyte layer thickness was maintained at ~10 μm. The cell was equipped with a standard 3-electrode configuration, controlled with a potentiostat and continuously flushed with the electrolyte (0.1 M K-P_i). $BiVO_4$ samples were illuminated from the back-side using a Xe lamp equipped with an optical fiber.

The XANES spectra, three scans per sample, were energy-calibrated, averaged and further analysed using the FDMNES package program using multiple scattering theory based on the muffin-tin approximation on the potential shape.[64,65] The muffin-tin radii were tuned to have a 10% overlap between the different spherical potentials. The Hedin–Lundqvist exchange potential was used. The XANES spectrum of a $BiVO_4$ crystal was calculated, considering in the calculation all the atoms surrounding the absorber V within a 7 Å radius sphere. The approximation of non-excited absorbing atoms was used, which better reproduces the experimental data. A similar calculation with the FEFF8 code[66] gave similar results. We have not considered the effect of the structural disorder in the XANES simulations. To simulate the XANES spectra, a core-hole broadening of 1.0 eV was used.

Impedance spectroscopy (IS)

IS measurements were carried out in the same set up configuration as the PEC measurements by applying a 20 mV AC signal and scanning in a frequency range between 1 MHz and 50 mHz, at different applied bias. The numerical fitting of the impedance data was carried out using the Zview software (Scribner Associates).

Scanning electron microscopy (SEM)

The morphology of thin films was investigated using SEM microscopy (JEOL JSM-6010LA instrument equipped with a tungsten hairpin filament). Samples were investigated in the secondary electron imaging mode (SEI), using an Everhart–Thornley type

detector. SEM images were collected using an accelerating voltage of 20 kV, at a working distance of 10 mm.

X-ray photoelectron spectroscopy (XPS)

XPS experiment was performed using the Thermo Scientific K-alpha apparatus equipped with an Al K-alpha X-ray Source and a Flood Gun. Parameters used for the measurements were: spot size of 400 mm, pass energy of 50 eV, energy step size of 0.1 eV, dwell time of 50 ms, 10 scans in the vicinity of the orbital binding energy of the elements of interest. XPS spectra were corrected for the C peak position.

Acknowledgements

We acknowledge the financial support of the Foundation for Fundamental Research on Matter (FOM TNW 10.327). This work has been done under the agenda of the BioSolarCells Consortium supported by the Dutch Ministry of Economic Affairs, Agriculture and Innovation. We acknowledge The Netherlands Organisation for Scientific Research (NWO) for financial support of the measurements at ESRF. We also thank financial support from the University Jaume I through the project P1·1B2011-50.

References

1 M. Grätzel, *Nature*, 2001, **414**, 338–344.
2 M. G. Walter, E. L. Warren, J. R. McKone, S. W. Boettcher, Q. Mi, E. A. Santori and N. S. Lewis, *Chem. Rev.*, 2010, **110**, 6446–6473.
3 D. G. Nocera, *Acc. Chem. Res.*, 2012, **45**, 767–776.
4 *Photoelectrochemical Hydrogen Production*, ed. R. van de Krol and M. Grätzel, Springer, US, Boston, MA, 2012, vol. 102.
5 R. van de Krol, Y. Liang and J. Schoonman, *J. Mater. Chem.*, 2008, **18**, 2311.
6 S. D. Tilley, M. Cornuz, K. Sivula and M. Grätzel, *Angew. Chem., Int. Ed.*, 2010, **49**, 6405–6408.
7 R. Solarska, A. Królikowska and J. Augustyński, *Angew. Chem., Int. Ed.*, 2010, **49**, 7980–7983.
8 K. Sayama, A. Nomura, T. Arai, T. Sugita, R. Abe, M. Yanagida, T. Oi, Y. Iwasaki, Y. Abe and H. Sugihara, *J. Phys. Chem. B*, 2006, **110**, 11352–11360.
9 A. Paracchino, V. Laporte, K. Sivula, M. Grätzel and E. Thimsen, *Nat. Mater.*, 2011, **10**, 456–461.
10 L. Han, F. F. Abdi, R. van de Krol, R. Liu, Z. Huang, H.-J. Lewerenz, B. Dam, M. Zeman and A. H. M. Smets, *ChemSusChem*, 2014, **7**, 2832–2838.
11 J. W. Ager III, M. Shaner, K. Walczak, I. D. Sharp and S. Ardo, *Energy Environ. Sci.*, 2015, **8**, 2811–2824.
12 S. Tokunaga, H. Kato and A. Kudo, *Chem. Mater.*, 2001, **13**, 4624–4628.
13 F. F. Abdi, N. Firet and R. van de Krol, *ChemCatChem*, 2013, **5**, 490–496.
14 D. K. Zhong, S. Choi and D. R. Gamelin, *J. Am. Chem. Soc.*, 2011, **133**, 18370–18377.
15 T. H. Jeon, W. Choi and H. Park, *Phys. Chem. Chem. Phys.*, 2011, **13**, 21392–21401.
16 F. F. Abdi and R. van de Krol, *J. Phys. Chem. C*, 2012, **116**, 9398–9404.
17 C. Ding, J. Shi, D. Wang, Z. Wang, N. Wang, G. Liu, F. Xiong and C. Li, *Phys. Chem. Chem. Phys.*, 2013, **15**, 4589–4595.
18 S. K. Choi, W. Choi and H. Park, *Phys. Chem. Chem. Phys.*, 2013, **15**, 6499–6507.
19 T. W. Kim and K. Choi, *Science*, 2014, **343**, 990–994.
20 M. Haro, C. Solis, V. M. Blas-Ferrando, O. Margeat, S. Ben Dhkil, C. Videlot-Ackermann, J. Ackermann, F. Di Fonzo, A. Guerrero and S. Gimenez, *ChemSusChem*, 2016, **9**, 3062–3066.
21 K. P. S. Parmar, H. J. Kang, A. Bist, P. Dua, J. S. Jang and J. S. Lee, *ChemSusChem*, 2012, **5**, 1926–1934.
22 P. M. Rao, L. Cai, C. Liu, I. S. Cho, C. H. Lee, J. M. Weisse, P. Yang and X. Zheng, *Nano Lett.*, 2014, **14**, 1099–1105.
23 Y. Pihosh, I. Turkevych, K. Mawatari, J. Uemura, Y. Kazoe, S. Kosar, K. Makita, T. Sugaya, T. Matsui, D. Fujita, M. Tosa, M. Kondo and T. Kitamori, *Sci. Rep.*, 2015, **5**, 11141.
24 F. F. Abdi, T. J. Savenije, M. M. May, B. Dam and R. van de Krol, *J. Phys. Chem. Lett.*, 2013, **4**, 2752–2757.
25 D. Eisenberg, H. S. Ahn and A. J. Bard, *J. Am. Chem. Soc.*, 2014, **136**, 14011–14014.
26 M. T. McDowell, M. F. Lichterman, J. M. Spurgeon, S. Hu, I. D. Sharp, B. S. Brunschwig and N. S. Lewis, *J. Phys. Chem. C*, 2014, **118**, 19618–19624.
27 B. J. Trześniewski and W. A. Smith, *J. Mater. Chem. A*, 2016, **4**, 2919–2926.
28 M. Gostein and L. Dunn, in 2011 37th IEEE Photovoltaic Specialists Conference, IEEE, 2011, pp. 003126–003131.
29 A. Listorti, C. Creager, P. Sommeling, J. Kroon, E. Palomares, A. Fornelli, B. Breen, P. R. F. Barnes, J. R. Durrant, C. Law and B. O'Regan, *Energy Environ. Sci.*, 2011, **4**, 3494.
30 F. J. Lim, Y. T. Set, A. Krishnamoorthy, J. Ouyang, J. Luther and G. W. Ho, *J. Mater. Chem. A*, 2015, **3**, 314–322.
31 C. Liu, J. Fan, X. Zhang, Y. Shen, L. Yang and Y. Mai, *ACS Appl. Mater. Interfaces*, 2015, **7**, 9066–9071.
32 F. Lin and S. W. Boettcher, *Nat. Mater.*, 2014, **13**, 81–86.
33 T. J. Mills, F. Lin and S. W. Boettcher, *Phys. Rev. Lett.*, 2014, **112**, 148304.
34 F. Lin, B. F. Bachman and S. W. Boettcher, *J. Phys. Chem. Lett.*, 2015, **6**, 2427–2433.
35 C. Du, X. Yang, M. T. Mayer, H. Hoyt, J. Xie, G. McMahon, G. Bischoping and D. Wang, *Angew. Chem., Int. Ed.*, 2013, **52**, 12692–12695.
36 C. Du, M. Zhang, J. Jang, Y. Liu, G. Liu and D. Wang, *J. Phys. Chem. C*, 2014, **118**, 17054–17059.
37 I. C. Man, H.-Y. Su, F. Calle-Vallejo, H. A. Hansen, J. I. Martínez, N. G. Inoglu, J. Kitchin, T. F. Jaramillo, J. K. Nørskov and J. Rossmeisl, *ChemCatChem*, 2011, **3**, 1159–1165.
38 X. Shi, I. Herraiz-Cardona, L. Bertoluzzi, P. Lopez-Varo, J. Bisquert, J. H. Park and S. Gimenez, *Phys. Chem. Chem. Phys.*, 2016, **18**, 9255–9261.
39 J. Reichman, *Appl. Phys. Lett.*, 1980, **36**, 574–577.
40 F. F. Abdi, N. Firet, A. Dabirian and R. van de Krol, *MRS Proc.*, 2012, **1446**, mrss12-1446-u02-05.

41 X. Yang, C. Du, R. Liu, J. Xie and D. Wang, *J. Catal.*, 2013, **304**, 86–91.
42 K. Sivula, *J. Phys. Chem. Lett.*, 2013, **4**, 1624–1633.
43 T. Li, J. He, B. Peña and C. P. Berlinguette, *Angew. Chem., Int. Ed.*, 2016, **55**, 1769–1772.
44 M. Mullet, V. Khare and C. Ruby, *Surf. Interface Anal.*, 2008, **40**, 323–328.
45 J. K. Cooper, S. Gul, F. M. Toma, L. Chen, P.-A. Glans, J. Guo, J. W. Ager, J. Yano and I. D. Sharp, *Chem. Mater.*, 2014, **26**, 5365–5373.
46 G. Wang, Y. Ling, X. Lu, F. Qian, Y. Tong, J. Z. Zhang, V. Lordi, C. Rocha Leao and Y. Li, *J. Phys. Chem. C*, 2013, **117**, 10957–10964.
47 D.-D. Qin, T. Wang, Y.-M. Song and C.-L. Tao, *Dalton Trans.*, 2014, **43**, 7691–7694.
48 A. Bianconi, *X-ray Absorption: Principles, Applications, Techniques of EXAFS, SEXAFS and XANES*, Wiley, New York, 1988.
49 D. K. Bediako, B. Lassalle-Kaiser, Y. Surendranath, J. Yano, V. K. Yachandra and D. G. Nocera, *J. Am. Chem. Soc.*, 2012, **134**, 6801–6809.
50 B. Klahr and T. Hamann, *J. Phys. Chem. C*, 2014, **118**, 10393–10399.
51 O. Zandi and T. W. Hamann, *J. Phys. Chem. Lett.*, 2014, **5**, 1522–1526.
52 L. Bertoluzzi, L. Badia-Bou, F. Fabregat-Santiago, S. Gimenez and J. Bisquert, *J. Phys. Chem. Lett.*, 2013, **4**, 1334–1339.
53 L. Bertoluzzi and J. Bisquert, *J. Phys. Chem. Lett.*, 2012, **3**, 2517–2522.
54 B. Klahr, S. Gimenez, F. Fabregat-Santiago, T. Hamann and J. Bisquert, *J. Am. Chem. Soc.*, 2012, **134**, 4294–4302.
55 B. Klahr, S. Gimenez, F. Fabregat-Santiago, J. Bisquert and T. W. Hamann, *J. Am. Chem. Soc.*, 2012, **134**, 16693–16700.
56 L. Badia-Bou, E. Mas-Marza, P. Rodenas, E. M. Barea, F. Fabregat-Santiago, S. Gimenez, E. Peris and J. Bisquert, *J. Phys. Chem. C*, 2013, **117**, 3826–3833.
57 S. Gimenez, H. K. Dunn, P. Rodenas, F. Fabregat-Santiago, S. G. Miralles, E. M. Barea, R. Trevisan, A. Guerrero and J. Bisquert, *J. Electroanal. Chem.*, 2012, **668**, 119–125.
58 Z. Zhang, C. Shao, L. Zhang, X. Li and Y. Liu, *J. Colloid Interface Sci.*, 2010, **351**, 57–62.
59 R. Yu, N. Xue, S. Huo, J. Li and J. Wang, *RSC Adv.*, 2015, **5**, 63502–63512.
60 Y. Zhang, Y. Guo, H. Duan, H. Li, C. Sun and H. Liu, *Phys. Chem. Chem. Phys.*, 2014, **16**, 24519–24526.
61 G. Liu, J. Shi, F. Zhang, Z. Chen, J. Han, C. Ding, S. Chen, Z. Wang, H. Han and C. Li, *Angew. Chem., Int. Ed.*, 2014, **53**, 7295–7299.
62 Y. Liang, T. Tsubota, L. P. A. Mooij and R. van de Krol, *J. Phys. Chem. C*, 2011, **115**, 17594–17598.
63 S. Nikitenko, A. M. Beale, A. M. J. van der Eerden, S. D. M. Jacques, O. Leynaud, M. G. O'Brien, D. Detollenaere, R. Kaptein, B. M. Weckhuysen and W. Bras, *J. Synchrotron Radiat.*, 2008, **15**, 632–640.
64 O. Bunău and Y. Joly, *J. Phys.: Condens. Matter*, 2009, **21**, 345501.
65 Y. Joly, *Phys. Rev. B: Condens. Matter Mater. Phys.*, 2001, **63**, 125120.
66 A. Ankudinov, B. Ravel, J. Rehr and M. Newville, *FEFFFIT manual within the FEFF project*, University of Washington, Seattle, USA, 1992-1999.